Journal of Solid State Chemistry 185 (2012) 72–75

Contents lists available at SciVerse ScienceDirect

Journal of Solid State Chemistry

journal homepage: www.elsevier.com/locate/jssc

Pressure-induced phase transition of Fe_2TiO_4: X-ray diffraction and Mössbauer spectroscopy

Ye Wu [a,b], Xiang Wu [a,b,*], Shan Qin [a,b]

[a] Key Laboratory of Orogenic Belts and Crustal Evolution, MOE, Peking University, Beijing 100871, China
[b] School of Earth and Space Sciences, Peking University, Beijing 100871, China

ARTICLE INFO

Article history:
Received 23 May 2011
Received in revised form
23 October 2011
Accepted 29 October 2011
Available online 7 November 2011

Keywords:
Ulvöspinel Fe_2TiO_4
High pressure
Phase transition
X-ray diffraction
Mössbauer spectroscopy

ABSTRACT

X-ray diffraction and Mössbauer spectroscopy were employed to investigate structural stability of Fe_2TiO_4 under high pressure. Measurements were performed up to about 24 GPa at room temperature using diamond anvil cell. Experimental results demonstrate that Fe_2TiO_4 undergoes a series of phase transitions from cubic ($Fd\bar{3}m$) to tetragonal ($I4_1/amd$) at 8.7 GPa, and then to orthorhombic structure ($Cmcm$) at 16.0 GPa. The high-pressure phase ($Cmcm$) of Fe_2TiO_4 is kept on decompression to ambient pressure. In all polymorphs of Fe_2TiO_4, iron cations present a high-spin ferrous property without electric charge exchange with titanium cations at high pressure supported by Mössbauer evidences.

1. Introduction

The solid solutions $Fe^{2+}_{1+x}Fe^{3+}_{2-2x}Ti_xO_4$ $(0 \le x \le 1)$ known as titanomagnetite are important minerals in nature because they are essential carriers of the magnetic signals in rocks, and material science due to diverse magnetic, electrical, and thermodynamic properties. All these properties depend on the concentration and distribution of Fe and Ti among sites of different symmetries in the structure. Therefore, many investigations have been carried out on crystal structure and cations distributions of titanomagnetites [1–8]. Titanomagnetites have a spinel-type structure, whose unit cell is faced-centered cubic (space group $Fd\bar{3}m$ and $Z=8$). Previous studies show that titanomagnetites can be described in three models as follows:

Akimoto model [8]

$$^{T}(Fe^{3+}_{1-x}Fe^{2+}_{x})^{O}(Fe^{2+}Fe^{3+}_{1-x}Ti_x)O_4 \ (0 \le x \le 1.0) \quad (1)$$

Néel–Chevallier model [9,10]:

$$^{T}(Fe^{3+})^{O}(Fe^{2+}_{1+x}Fe^{3+}_{1-2x}Ti_x)O_4 \ (0 \le x \le 0.5) \text{ and } ^{T}(Fe^{3+}_{2-2x}Fe^{2+}_{2x-1})^{O}(Fe^{2+}_{2-x}Ti_x)O_4 \ (0.5 \le x \le 1.0) \quad (2)$$

O'Reilly and Banerjee model [2]:

$$^{T}(Fe^{3+})^{O}(Fe^{2+}_{1+x}Fe^{3+}_{1-2x}Ti_x)O_4 \ (0 \le x \le 0.2), ^{T}(Fe^{3+}_{1.2-x}Fe^{2+}_{x-0.2})\ ^{O}(Fe^{2+}_{1.2}Fe^{3+}_{0.8-x}Ti_x)O_4 \ (0.2 \le x \le 0.8) \text{ and } ^{T}(Fe^{3+}_{2-2x}Fe^{2+}_{2x-1})^{O}(Fe^{2+}_{2-x}Ti_x)O_4 \ (0.8 \le x \le 1.0), \quad (3)$$

where T and O denote tetrahedral and octahedral sites, respectively. Deviations from this model can be explained by an electron exchange reaction:

$$^{T}Fe^{2+} + {}^{O}Fe^{3+} \rightarrow {}^{T}Fe^{3+} + {}^{O}Fe^{2+} \quad (4)$$

which causes $^{O}Fe^{2+} \neq 1$ and $^{T}Fe^{2+}/Ti \neq 1$ [1].

In relation to the composition effect, the end-member components—Fe_3O_4 and Fe_2TiO_4 are focused on the crystal chemistry and physical property at various external conditions, such as temperature, pressure, and magnetic field. A high-pressure Fe_3O_4 phase (h-Fe_3O_4) is reported with $CaMn_2O_4$-type structure ($Pbcm$) at about 24 GPa and 823 K [11]. However, the $CaTi_2O_4$-type ($Bbmm$) phase is proposed for the h-Fe_3O_4 which presents metallic in the later studies [12]. For Fe_2TiO_4, phase transition from cubic ($Fd\bar{3}m$) to tetragonal ($I4_1/amd$) occurs below the Curie temperature T_C (T_C= 142 K) studied by magnetism measurement and neutron diffraction [13]. Under high pressure, cubic phase of Fe_2TiO_4 transforms into tetragonal phase ($I4_1/amd$) at 9 GPa, and then into post-spinel phase ($Cmcm$) at 12 GPa [14]. In addition, cations distributions of Fe_2TiO_4 at various temperatures have been investigated using Mössbauer spectroscopy (MS) by Schmidbauer [15], whose results show that Fe^{2+} cations in O sites are replaced by Fe^{3+} cations and cation vacancies at low temperature according to the formula:

$$3Fe^{2+} \rightarrow 2Fe^{3+} + \square (\square = \text{vacancy}) \quad (5)$$

To our best knowledge, no literatures have been published about the valance state and spin state of iron ions, cations distributions in O and T sites of Fe_2TiO_4 under high pressure. Consequently, our works aim to explore the structural stability

* Corresponding author at: School of Earth and Space Sciences, Peking University, Beijing 100871, China. Fax: +86 10 62752996.
E-mail address: xiang.wu@pku.edu.cn (X. Wu).

0022-4596/$ - see front matter © 2011 Elsevier Inc. All rights reserved.
doi:10.1016/j.jssc.2011.10.045

and iron electron configuration of Fe_2TiO_4 at high pressure by synchrotron radiation X-ray diffraction (XRD) and MS combined with diamond anvil cell (DAC).

2. Experiments

The Fe_2TiO_4 ulvöspinel sample was synthesized by standard solid-state reaction. Stoichiometric amounts of $^{56}Fe_2O_3$ (99.998%), $^{57}Fe_2O_3$ (95%) and TiO_2 (99.998%) (mole ratios, 0.34:0.66:1) were mixed and ground together with ethanol in an agate mortar. The mixtures were compressed into pellets with a diameter of 3 mm. These pellets were heated in an open Pt capsule at 1300 °C for 24 h in CO–CO_2 gas mixtures corresponding to oxygen fugacity ($fO_2=10^{-11}$), and then quenched to ambient conditions. The product was examined *ex situ* by the JEOL JXA-8200 electron microprobe with an accelerating voltage of 15 kV and a beam current of 15 nA. The sample was also characterized using XRD, which confirmed a single phase ($Fd\bar{3}m$) without any impurities. Four-pin modified Merrill–Bassett type DAC was applied in high-pressure experiments. For XRD experiments, the sizes of culets were diameters of 300 μm; a 120 μm—diameter hole was drilled in the pre-indented 50 μm stainless steel T301 gasket; LiF was used as pressure-transmitting medium and pressure calibration [16]. While for MS experiments, the diamond culets were the diameter of 500 μm; the sample chamber was a 250 μm—diameter hole with the 50 μm height in Re gasket; pressure-transmitting medium was Ne; ruby was used as pressure calibration [17].

XRD data were collected at the Shanghai Synchrotron Radiation Facility (SSRF, Shanghai, China) on beam line 15U, with a focused monochromatic beam ($\lambda=0.6889$ Å, beam size 5×10 μm^2) and a Mar CCD detector. The distance from detector to sample was about 168 mm, and collection time of each pattern was 20 s. In order to obtain conventional one-dimensional diffraction spectra, the two-dimensional images of the CCD camera were integrated using the Fit2D program. *In situ* ^{57}Fe MS of Fe_2TiO_4 at high pressure were measured in a transmission mode on a constant acceleration Mössbauer spectrometer using a high specific activity ^{57}Co point source in a Rh matrix. The velocity scale was calibrated relative to a 25 μm-thick α-Fe foil. Collection time for each spectrum was about 10 h. MS spectra were fitted to Lorentzian line shapes using a least-square fitting program NORMOS-90 written by R. A. Brand (distributed by Wissenschaftliche Elektronik GmbH, Germany), where equal intensities of the quadrupole components were assumed in the fitting procedure.

3. Results and discussion

The XRD study was performed up to about 24 GPa at room temperature. And then the pressure was relaxed to ambient pressure. Fig. 1 shows several typical XRD patterns along with compression (a–e) and decompression (e and f). At ambient pressure, all diffraction peaks can be indexed to Fe_2TiO_4 ($Fd\bar{3}m$) and LiF ($Fm3m$). At 8.7 GPa, the (220) peak of Fe_2TiO_4 was splitted into two peaks (Fig. 1b), which became more obvious with increasing pressure, such as at 14.7 GPa (Fig. 1c). The appearance of new peaks in Fig. 1b and c demonstrate that Fe_2TiO_4 undergoes a phase transition, where the high-pressure phase was assigned to tetragonal phase ($I4_1/amd$). At about 16 GPa, diffraction peaks of tetragonal phase disappeared such as the double peaks around 2θ of 13.5°, and at the same time, some new peaks emerged, seen one typical pattern Fig. 1d. The new phase is the post-spinel phase with $CaTi_2O_4$-type structure ($Cmcm$). The phase-transition sequence of Fe_2TiO_4 observed here is consistent with that of previous study [14]. On decompression from 24 GPa to

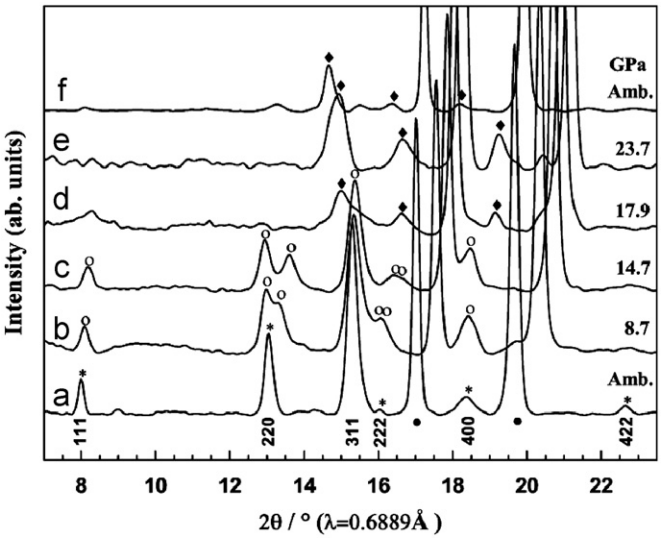

Fig. 1. Selected XRD patterns of Fe_2TiO_4 during compression (a–e) and at ambient pressure following decompression (f). Backgrounds were subtracted from the original data and all data were normalized. Diffraction peaks of Fe_2TiO_4 polymorphs are marked by symbol * for cubic spinel, ○ for tetragonal spinel, ♦ for orthorhombic postspinel, while symbol ● represents those of LiF.

0.0001 GPa (Fig. 1e and f), the post-spinel phase is kept with a metastable property at ambient conditions.

Crystal structures of the above three polymorphs of Fe_2TiO_4 are illustrated in previous work [14]. The ideal cubic ulvöspinel is based on a cubic-close-packed oxygen lattice with Fe and Ti occupying one-eighth of the available *T* sites and one-second of the available *O* sites; half of Fe^{2+} cations and all Ti^{4+} cations occupy *O* sites and remaining Fe^{2+} cations occupy *T* sites. In tetragonal phase, cations occupy the same sites with cubic phase; [FeO_6] or [TiO_6] octahedrons have a small distortion. In orthorhombic phase, there are two different cation sites, where half of Fe^{2+} cations and all Ti^{4+} occupy *O* sites and the rest Fe^{2+} is located in a new sixfold-coordinated site described as asymmetric trigonal prism (marked as TP).

In situ high pressure MS data were collected up to 19.6 GPa. Twelve spectra were collected with increasing pressure. Several typical spectra are shown in Fig. 2. All spectra can be fitted using two doublets attributed to Fe^{2+} components without any Fe^{3+} component. Previous studies adapted a fitting model with four quadrupole doublets due to variable next-nearest cation distributions at the resonance nuclei [18]. For our work, using fitting models with four doublets resulted in considerably poorer fits, so we neglected the next-nearest cation effect. In cubic and tetragonal phases, one doublet with large quadrupole splitting ΔE_Q we assign as $^{O}(Fe^{2+})$; the other we assign as $^{T}(Fe^{2+})$ (Fig. 2a–c), and in orthorhombic phase, $^{O}(Fe^{2+})$ is the doublet with large ΔE_Q and $^{TP}(Fe^{2+})$ is the other one with small ΔE_Q (Fig. 2d). During the whole pressure range, the Fe^{2+} is in high-spin state. All Fe^{2+} hyperfine parameters (isomer shift δ, ΔE_Q and the full width at half maximum Γ) of Fe_2TiO_4 at various pressures are listed in Table 1 and plotted in Fig. 3 for comparison.

For $^{O}(Fe^{2+})$ component and $^{T}(Fe^{2+})$ component of cubic phase Fe_2TiO_4 at 1.3 GPa, the isomer shift δ are 0.867 mm/s and 0.898 mm/s, respectively, which are consistent with that of the previous studies at ambient conditions ($\delta=1.0$ mm/s) [18]. Both δ of $^{O}(Fe^{2+})$, $^{T}(Fe^{2+})$ and $^{TP}(Fe^{2+})$ decrease with increasing pressure (Fig. 3a). For the same source, δ can be described as $\delta=\alpha(\rho(0)—c)$, where α is the calibration constant with minus value; $\rho(0)$ and c stand for the *s* electron charge densities at the nuclei in the absorber and the source, respectively, and c is a constant.

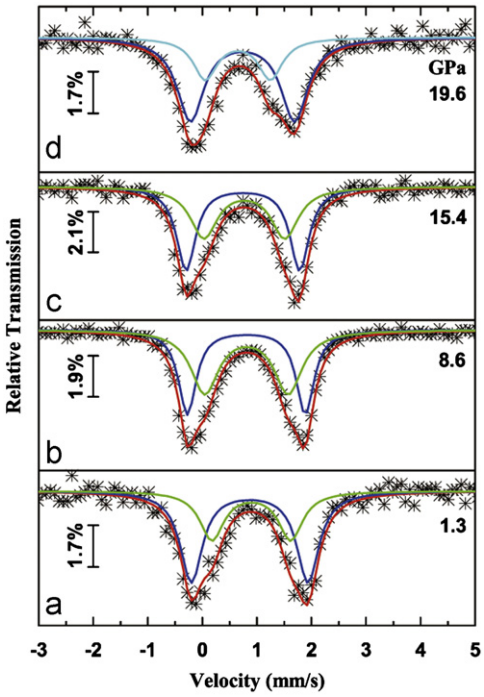

Fig. 2. Typical ^{57}Fe Mössbauer spectra of Fe_2TiO_4 at high pressure. The asterisks show experimental data. The red line is the superposition of the two quadrupole doublets; the blue line for $^{O}(Fe^{2+})$; the green line for $^{T}(Fe^{2+})$ and cyan line for $^{TP}(Fe^{2+})$. (For interpretation of the references to color in this figure legend, the reader is referred to the web version of this article.)

Table 1
Fe^{2+} hyperfine parameters in Fe_2TiO_4 at various pressures.[a]

P (GPa)	$^{O}(Fe^{2+})$			$^{T}(Fe^{2+})/^{TP}(Fe^{2+})$		
	δ (mm/s)	ΔE_Q (mm/s)	Γ (mm/s)	δ (mm/s)	ΔE_Q (mm/s)	Γ (mm/s)
1.3	0.867(08)	2.14(4)	0.49(5)	0.898(17)	1.44(9)	0.54(8)
2.5	0.853(09)	2.18(3)	0.35(6)	0.855(13)	1.53(8)	0.58(6)
3.7	0.846(11)	2.11(3)	0.45(4)	0.831(12)	1.36(7)	0.49(8)
4.7	0.848(08)	2.22(3)	0.37(6)	0.838(12)	1.58(8)	0.64(6)
6.5	0.825(10)	2.22(3)	0.29(7)	0.816(11)	1.66(8)	0.66(5)
8.6	0.806(04)	2.16(1)	0.39(2)	0.810(03)	1.53(4)	0.61(3)
10.3	0.785(06)	2.19(2)	0.36(4)	0.810(08)	1.62(6)	0.61(4)
11.8	0.782(04)	2.18(2)	0.39(3)	0.795(07)	1.56(5)	0.61(3)
13.6	0.756(05)	2.13(2)	0.38(3)	0.779(09)	1.55(7)	0.60(5)
15.4	0.743(06)	2.08(3)	0.42(5)	0.771(13)	1.48(8)	0.60(6)
17.2	0.737(06)	2.02(4)	0.47(4)	0.748(12)	1.38(9)	0.59(7)
19.6	0.736(10)	1.91(4)	0.60(5)	0.651(21)	1.19(7)	0.54(8)

[a] Numbers in parentheses represent errors in the last digit.

Pressure leads to compression of *s* orbit, and *s* electron charge density increases. Consequently, δ decrease with increasing pressure.

Quadrupole splitting of $^{O}(Fe^{2+})$ is larger than that of $^{T}(Fe^{2+})$ and $^{TP}(Fe^{2+})$ (Fig. 3b), because a larger coordination number leads to a higher quadrupole splitting. ΔE_Q in *O* sites increases with octahedron distortions from cubic phase to tetragonal phase (from 2.14 mm/s to 2.22 mm/s), and then decreases from tetragonal phase to orthorhombic phase (from 2.22 mm/s to 1.91 mm/s). The quadrupole splitting for high spin Fe^{2+} in octahedral coordination could be $\Delta E_Q = \Delta E_Q(0)\alpha^2 F(\Delta_1, \Delta_2, \lambda_0, \alpha^2, T)$, where $\Delta E_Q(0)$ is the maximum possible value of the quadrupole splitting, F is the reduction function whose value is given by perturbation theory, Δ_1 and Δ_2 are the two lowest splitting of the crystal-field levels, α^2 is a covalence factor, λ_0 is a spin–orbit

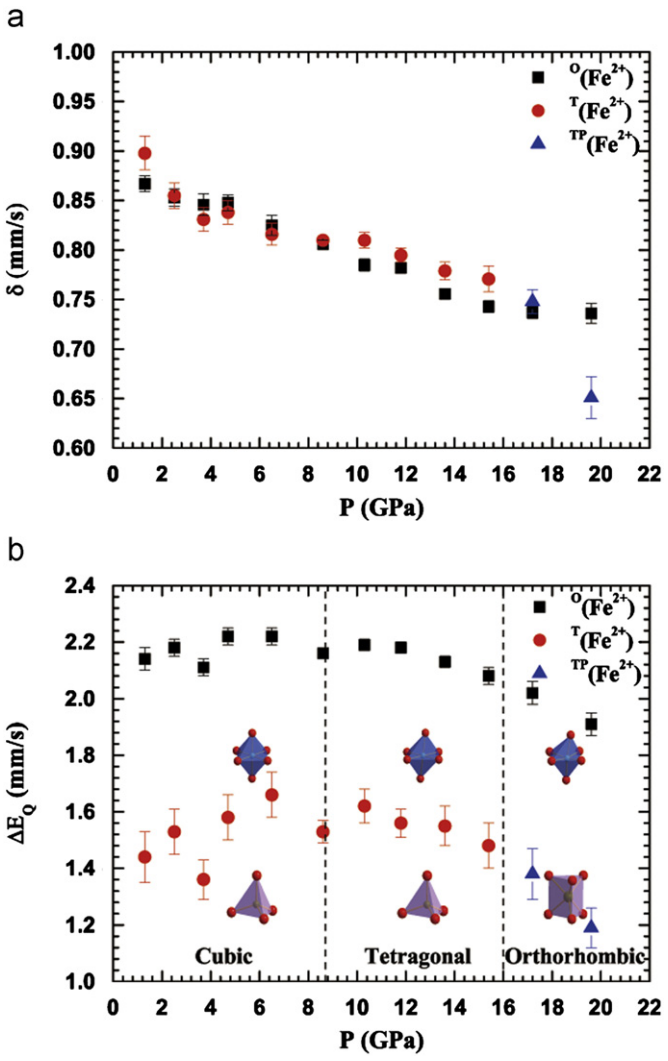

Fig. 3. Isomer shift (δ) and quadrupole splitting (ΔE_Q) of $^{O}(Fe^{2+})$, $^{T}(Fe^{2+})$ and $^{TP}(Fe^{2+})$ as a function of pressure marked as (a) and (b), respectively. Solid square, circle and triangle represent $^{O}(Fe^{2+})$, $^{T}(Fe^{2+})$ and $^{TP}(Fe^{2+})$, respectively. Inset in (b): blue [FeO_6] octahedron, lavender [FeO_4] tetrahedron and [FeO_6] trigonal prism, central atom is Fe atom and red ball is O atom. (For interpretation of the references to color in this figure legend, the reader is referred to the web version of this article.).

coupling constant, and T is the absolute temperature [19]. The roles of α^2 and λ_0 on the quadrupole splitting are neglected for simplicity. Thus, ΔE_Q is described to be ΔE_Q (0)$F(\Delta_1, \Delta_2, T)$. In general, the values of Δ_1 and Δ_2 can be used to express the octahedral distortion. Ingalls demonstrated that the quadrupole splitting increases very rapidly with increasing octahedral distortion at small distortion, and reaching a maximum [19]. For a larger octahedral distortion from tetragonal to orthorhombic, ΔE_Q of $^{O}(Fe^{2+})$ decreases with increasing octahedral distortion. Fig. 3b presents that the tendency of ΔE_Q for $^{O}(Fe^{2+})$ coincides with Ingalls' result [19]. As for $^{T}(Fe^{2+})$ and $^{TP}(Fe^{2+})$, ΔE_Q decreases with increasing distortions of coordination polyhedron. ΔE_Q of $^{T}(Fe^{2+})$ changes a little from cubic to tetragonal structure as both of their coordination polyhedrons are tetrahedrons (ΔE_Q= 1.44 mm/s at 1.3 GPa and ΔE_Q=1.48 mm/s at 15.4 GPa). ΔE_Q of $^{TP}(Fe^{2+})$ decreases with pressure increasing. Besides coordination number, ΔE_Q is relative to symmetry of polyhedron. Quadrupole splitting decreases with larger distortion of polyhedron. In a word, the structural information obtained from MS is consistent with that from XRD.

The evaluation of the relative abundances of $^{O}(Fe^{2+})$, $^{T}(Fe^{2+})$ and $^{TP}(Fe^{2+})$ from the MS area could not be determined due to the very thick absorber made of ~90% ^{57}Fe isotope. This can be verified from the larger values of the full width at half maximum Γ. Also, the hyperfine parameters were obtained by varied fitting strategies, so the errors of the area ratios are large. And at higher pressure the peak area are inconclusive or ineffective because the Mössbauer signals from $^{O}(Fe^{2+})$ and $^{T}(Fe^{2+})/^{TP}(Fe^{2+})$ were inextricable. Even so, combining previous studies with our MS results, Fe^{2+} of Fe_2TiO_4 are attributed to *O* sites and *T*/*TP* sites on average. One half of Fe^{2+} occupy all *T* or *TP* sites, and the remaining Fe^{2+} together with Ti^{4+} occupy *O* sites [14].

Yamanaka et al. analyzed the phase transition of cubic–to–tetragonal is related to the presence of Jahn–Teller Fe^{2+} ions in the tetrahedral site [14]. A low crystal-field stabilization energy (CFSE) of tetrahedral Fe^{2+} results in the Jahn–Teller transition. Fe^{2+} has six 3*d* electrons with two different spin states. For Fe^{2+} at low-spin state, T_{2g} orbit is full-filled and the Jahn–Teller distortions will disappear. High-spin Fe^{2+} due to asymmetric electronic cloud distribution of 3*d* orbit has the Jahn–Teller effect [20]. However, XRD results could not give direct evidence about iron electrical structure change (valence state and spin state). Our MS results directly demonstrate that iron in tetragonal site presents ferrous with high-spin state, meaning that the Jahn–Teller effect may exist in Fe_2TiO_4 at high pressure. In addition, the evidence of no Fe^{3+} indicates no electron exchange between Fe^{2+} and Ti^{4+}. Seda and Hearne have reported that pressure induced intervalence charge transfer away from the ferrous sites: $Fe^{2+}+Ti^{4+}\rightarrow Fe^{3+}+Ti^{3+}$ in natural ilmenite ($FeTiO_3$) minerals [21]. However, pressure induced intervalence charge transfer did not occur in stoichiometric synthesized Fe_2TiO_4. The electronic structures of cations are stable along with phase transition of Fe_2TiO_4 under high pressure.

4. Conclusions

High pressure XRD and MS experiments have been carried out at room temperature on stoichiometric synthesized Fe_2TiO_4. The XRD results show that phase transitions—from cubic spinel to tetragonal spinel and then to orthorhombic post-spinel occur at 8.7 GPa and 16 GPa, respectively, in agreement with previous high pressure studies [14]. The orthorhombic structure of Fe_2TiO_4 is preserved up to about 24 GPa. On decompression, the orthorhombic phase can be preserved at ambient conditions. The results of MS show that iron ions are high-spin ferrous irons during whole pressure range. No electron exchange occurs between Fe^{2+} and Ti^{4+}. For cubic spinel and tetragonal spinel, half of Fe^{2+} cations occupy *T* sites, and the remaining Fe^{2+} cations together with Ti^{4+} occupy *O* sites. As for orthorhombic phase, Fe^{2+} cations occupy asymmetric trigonal prisms and half of octahedrons, other *O* sites are occupied by Ti^{4+}.

Acknowledgments

The synchrotron radiation experiments were performed at the SSRF, Shanghai (Proposal no. 10sr0140). X. Wu and S. Qin are grateful for the financial support of the National Natural Science Foundation of China (Grant no. 41072027). The authors would like to thank L. Dubrovinsky and C. McCammon for their assistances in XRD and MS experiments.

References

[1] F. Bosi, U. Halenius, H. Skogby, Am. Mineral. 94 (2009) 181–189.
[2] W. O'Reilly, S.K. Banerjee, Phys. Lett. 17 (1965) 237–238.
[3] A.A. Cristóbal, E.F. Aglietti, M.S. Conconi, J.M.Porto López, Mater. Chem. Phys. 111 (2008) 341–345.
[4] H.H. Hamdeh, K. Barghout, J.C. Ho, P.M. Shand, L.L. Miller, J. Magn. Magn. Mater. 191 (1999) 72–78.
[5] J.B. O'Donovan, W. O'Reilly, Phys. Chem. Miner. 5 (1980) 235–243.
[6] B.A. Wechsler, D.H. Lindsley, C.T. Prewitt, Am. Mineral. 69 (1984) 754–770.
[7] Z. Kakol, J. Sabol, J.M. Honig, Phys. Rev. B 43 (1991) 649–654.
[8] S. Akimoto, J. Geomagn. Geoelectr. 6 (1954) 1–14.
[9] L. Néel, Adv. Phys. 4 (1955) 191–243.
[10] R. Chevallier, J. Bolfa, S. Mathieu, B. Soc. Fr. Mineral. Crist. 78 (1955) 307–346.
[11] Y.W. Fei, D.J. Frost, H.K. Mao, C.T. Prewitt, D. Häusermann, Am. Mineral. 84 (1999) 203–206.
[12] L.S. Dubrovinsky, N.A. Dubrovinskaia, C. McCammon, G.K. Rozenberg, R. Ahuja, J.M. Osorio-Guillen, V. Dmitriev, H.-P. Weber, T.L. Bihan, B. Johansson, J. Phys.—Condens. Matter 15 (2003) 7697–7706.
[13] I. Yoshikazu, S. Yashuhiko, Phys. Rev. Lett. 26 (1971) 1335–1338.
[14] T. Yamanaka, T. Mine, S. Asogawa, Y. Nakamoto, Phys. Rev. B 80 (2009) 1–10.
[15] E. Schmidbauer, Phys. Chem. Miner. 14 (1987) 533–541.
[16] J. Liu, L. Dubrovinsky, T.B. Ballaran, W. Crichton, High Pressure Res. 27 (2007) 483–489.
[17] H.K. Mao, J. Xu, P.M. Bell, J. Geophys. Res. 91 (1986) 4673–4676.
[18] F. Bosi, U. Halenius, H. Skogby, Am. Mineral. 93 (2008) 1312–1316.
[19] R. Ingalls, Phys. Rev. 133 (1964) A787–A795.
[20] H.A. Jahn, E. Teller, P. Roy, Soc. Lond. A Mat 161 (1937) 220–235.
[21] T. Seda, G.R. Hearne, J. Phys.: Condens. Matter 16 (2004) 2707–2718.